# THE COUPLED BOUNDARY LAYERS AND AIR-SEA TRANSFER EXPERIMENT IN LOW WINDS (CBLAST-LOW)

BY JAMES EDSON, TIMOTHY CRAWFORD*, JERRY CRESCENTI, TOM FARRAR, NELSON FREW, GREG GERBI, COSTAS HELMIS, TIHOMIR HRISTOV, DJAMAL KHELIF, ANDREW JESSUP, HAF JONSSON, MING LI, LARRY MAHRT, WADE MCGILLIS, ALBERT PLUEDDEMANN, LIAN SHEN, ERIC SKYLLINGSTAD, TIM STANTON, PETER SULLIVAN, JIELUN SUN, JOHN TROWBRIDGE, DEAN VICKERS, SHOUPING WANG, QING WANG, ROBERT WELLER, JOHN WILKIN, ALBERT WILLIAMS, D.K.P. YUE, AND CHRIS ZAPPA

**AFFILIATIONS**: EDSON – University of Connecticut, Avery Point, Groton, Connecticut; CRESCENTI – FPL Energy, Juno Beach, Florida; FARRAR, FREW, GERBI, PLUEDDEMANN, TROWBRIDGE, WELLER, AND WILLIAMS – Woods Hole Oceanographic Institution, Woods Hole, Massachusetts; HELMIS – University of Athens, Athens, Greece; HRISTOV AND SHEN – Johns Hopkins University, Baltimore, Maryland; KHELIF – University of California, Irvine, California; JESSUP – Applied Physics Laboratory, University of Washington, Seattle, Washington; JONSSON – CIRPAS, Monterey, California; LI – University of Maryland, Center for Environmental Sciences, Cambridge, Maryland; MAHRT, SKYLLINGSTAD, AND VICKERS, Oregon State University, Corvallis, Oregon; MCGILLIS AND ZAPPA – Lamont Doherty Earth Observatory, Columbia University, Palisades, New York; STANTON AND Q. WANG – Naval Postgraduate School, Monterey, California; SULLIVAN AND SUN, National Center for Atmospheric Research, Boulder, Colorado; S. WANG – Naval Research Laboratory, Monterey, California; WILKIN – Rutgers University, New Brunswick, New Jersey; YUE – Massachusetts Institute of Technology, Cambridge, Massachusetts.
**CORRESPONDING AUTHOR**: James Edson, University of Connecticut, Avery Point, Department of Marine Sciences, 1080 Shennecosset Road, Groton, CT 06340 E-mail: james.edson@uconn.edu

**Observations from a suite of platforms deployed in the coastal ocean south of Martha's Vineyard are being combined with numerical models and simulations to investigate the processes that couple the atmosphere and ocean in low to moderate wind conditions.**

The need to better understand and model the interdependence of the ocean and atmosphere has long been recognized in the climate and weather communities. Work has been carried out to investigate how the upper ocean responds to the atmosphere, leading to 1-D models of upper ocean response to the atmosphere (e.g., Kraus and Turner, 1967; Price et al., 1986) and more recently to fully three dimensional (3-D) ocean boundary layer (OBL) models employing closure schemes similar to those used in the atmospheric boundary layer (ABL; e.g. Mellor and Yamada, 1982; Large et al., 1994). However, progress on fully two-way coupled models has been slower, particularly on shorter, weather-related, timescales.

There are a number of reasons for this, e.g., the dynamics of the coupled marine boundary layers are driven by a myriad of processes (Fig. 1) that impact the exchange of momentum, heat and mass. However, the parameterizations required to simulate these processes contain too much uncertainty, and oceanographic models of the ocean surface are not sufficiently advanced to provide the necessary surface boundary conditions. Additionally, observations of the marine environment lack the necessary temporal and spatial resolution required to initialize these models. As a result, there has been insufficient evidence that the inclusion of a dynamic ocean would improve 3-5 day atmospheric forecasts.

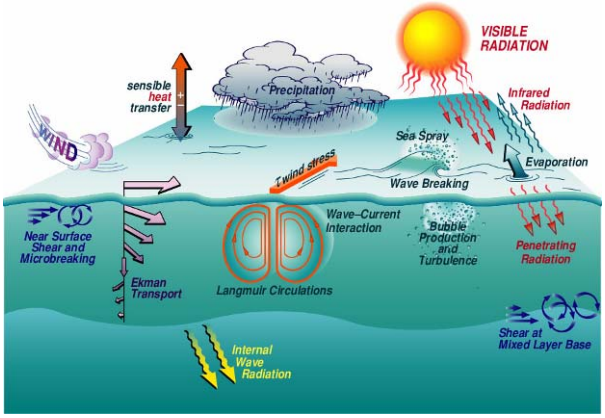


**Figure 1.** A few of the physical processes governing air-sea exchange across the coupled boundary layers.

Now, however, there is increasing evidence that fully coupled models can often improve marine forecasts over shorter time scales. This is true in coastal regimes where air-land-sea contrasts drive mesoscale atmospheric circulations, fog formation, coastal upwelling, and tidal mixing. This is also true of hurricane forecasts, where accurate predictions of the heat, mass and momentum exchange are crucial to accurately predict the intensity of the storm. All of these predictions rely on accurate estimates of the sea-surface temperature at temporal and spatial resolution that are often not provided by satellite observations, particularly near the coastline and in severe weather. Progress now underway to improve coupled models stems from 1) significant improvements in ocean models over the past decade and 2) observing initiatives that provide data needed to initialize these models and assess the success of different parameterizations. This article and its companion articles in this issue focus on a recent program designed to improve coupled models in both low and extreme wind conditions.

**CBLAST.** The Coupled Boundary Layer and Air-Sea Transfer (CBLAST) program was a major Office of Naval Research (ONR) sponsored investigation to look at two extremes of the marine environment where coupled ocean-atmosphere processes have a clear impact on both boundary layers. At one extreme, investigators in the CBLAST-Hurricane component are attempting to improve hurricane intensity forecasts and our understanding of the ocean's response as described in the companion articles by Black et al. (2006) and Chen et al. (2006).

CBLAST-LOW was designed to investigate coupled boundary layer (CBL) processes at the low-wind extreme where the processes are often driven or strongly modulated by buoyant forcing. The focus was on conditions ranging from negligible wind stress, where buoyant forcing dominates, up to wind speeds where wave breaking and Langmuir circulations play a significant role in the exchange processes. Additionally, as CBLAST-LOW developed, it became apparent that additional wave-driven processes could not be ignored, including the impact of ocean swell from distant storms on coupled boundary layer structure.

The goal of CBLAST-LOW is therefore to improve our understanding of the processes that couple the marine boundary layers under these conditions using observations, numerical simulations and models. The ultimate goal is to incorporate new and/or improved parameterization of these processes in coupled models to improve marine forecasts of wind, waves and currents. The article begins by briefly describing the region where CBLAST-LOW was conducted. It then describes the observational and modeling components and provides examples of how these components are being combined to meet the CBLAST objectives.

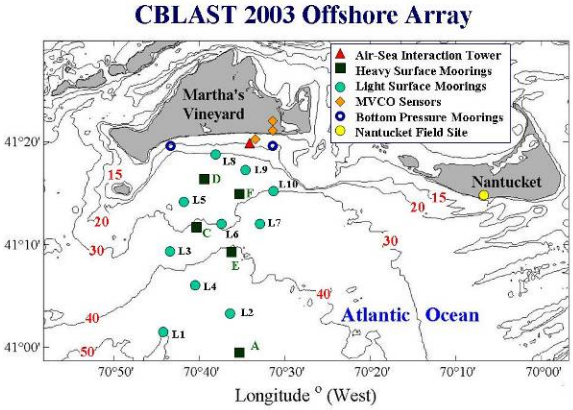


**Figure 2.** A diagram of the CBLAST region showing the location of the Nantucket field site, surface moorings, ASIT, subsurface moorings, and MVCO sensors deployed during the IOP in the summer 2003. The lines indicate the bathymetry and the isobaths are given in meters using red numbers.

**SITE DESCRIPTION.** CBLAST-LOW was conducted during intensive operating periods (IOPs) in the summers of 2001 through 2003 in the Atlantic Ocean south of Martha's Vineyard (Fig. 2). The CBLAST-LOW

region is bounded to the north by Martha's Vineyard and Nantucket, with shoals in between. Noman's Island to the west and Wasque Shoals to the east limit the fetch, and thereby wave development, for wind from those directions near the coastline of Martha's Vineyard. However, the fetch is essentially infinite for southerly wind directions.


**Figure 3.** A schematic representation of the MVCO showing the location of the meteorological mast, seanode, and ASIT. The cutout shows the actual location of these elements on the South shore of Martha's Vineyard.

Continuous observations of the ocean and atmosphere are maintained at the Martha's Vineyard Coastal Observatory (MVCO), which includes a meteorological mast on the beach and a bottom-mounted seanode (Fig. 3). These platforms support sensors that have operated continuously (with the exception of maintenance activities) since 2001. Therefore, the time series from the MVCO provides the beginning of a local climatology from 5 years of continuous operation, which can be compared with individual years. For example, Figs. 4a and 5a provide histograms of the wind speeds and wind directions, respectively, measured at the meteorological mast during July and August.

The accumulated data indicate that the predominant winds are from the SW with wind speeds typically reaching 2-6 m/s. As such, the wind directions are predominately from the open ocean. The main IOP in the summer of 2003 was fairly typical (Figs. 4b and 5b), with wind speeds and directions that were slightly lighter and more southerly, respectively, than the composite.

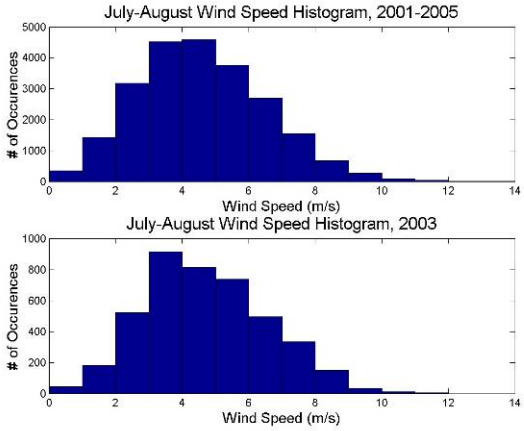


**Figure 4.** Histograms of wind speed data collected at the MVCO during the months of July and August. The upper panel shows the composite of all data taken from 2001 to 2005. The lower panel uses data from 2003.

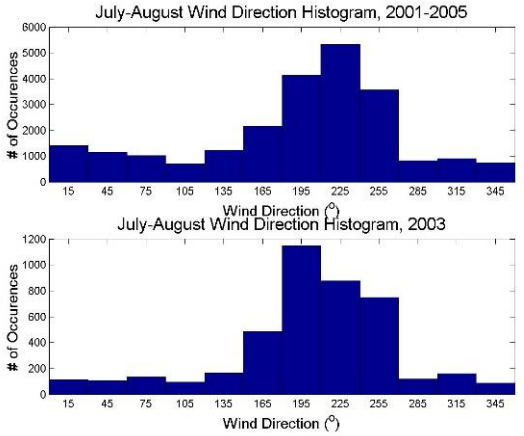


**Figure 5.** Histograms of wind direction data collected at the MVCO during the months of July and August. The upper panel shows the composite of all data taken from 2001 to 2005. The lower panel uses data from 2003.

Oceanic variables are also continuously available from the MVCO seanode. The currents in the CBLAST region are dominated by tides and fluctuate between 0-0.5 m/s. The sea surface elevation changes by approximately ±0.5 m during a tidal cycle. The tidally averaged mean surface currents are O(10 cm/s) and flow from east to west near

the coast of Martha's Vineyard. The sea temperature measured at a depth of 11-m averaged 19.0°C during the 5 years period and 18.9°C during the 2003 IOP.

**OBSERVATIONAL COMPONENTS**: CBLAST-LOW deployed and extensive array of observational components during the IOPs. A wide range of temporal and spatial scales was sampled using an array of fixed and mobile platforms; including an offshore tower, surface moorings, aircraft, ships, rawinsondes, satellites, and the MVCO. The periods of operation for the various platforms during the 2001-2003 IOPs are provided as timelines at the CBLAST-LOW website: http://www.whoi.edu/science/AOPE/dept/CBLAST/low/timelines.html. Data collected from these platforms is also available from the CBLAST-LOW website at http://www.whoi.edu/science/AOPE/dept/CBLAST/low/data.html.

***Air-Sea Interaction Tower***. Marine researchers have long sought stable ocean platforms that would allow studies of turbulent air-sea exchanges. A primary technological objective of the CBLAST-LOW program was to build an Air-Sea Interaction Tower (ASIT) to enable long-duration studies of the processes on both sides of the air-sea interface. ASIT is a low profile, fixed structure that minimizes flow distortion and removes the need for motion correction. It is located 3.2 km south of Martha's Vineyard in 15-m water depth (Figs. 2 and 3), and was completed in the summer of 2002. It is attached by cable to the MVCO, which provides power (4 kW) and a high-bandwidth (1 Gbyte) data link (Austin et al., 2002).

Atmospheric sensors at fixed heights and on a vertical profiler were deployed on the ASIT during the 2003 IOP to directly measure the vertical exchange of momentum, heat and moisture that couple the boundary layers. The air-side components included sensors to measure the mean and turbulent wind velocity, air temperature, specific humidity, and pressure; as well as precipitation, solar and infrared radiation, sea surface temperature, and wave height. (Fig. 6a). The ASIT is exposed to infinite fetch for wind directions from 140° to 250° and is fetch limited from other directions as described above.

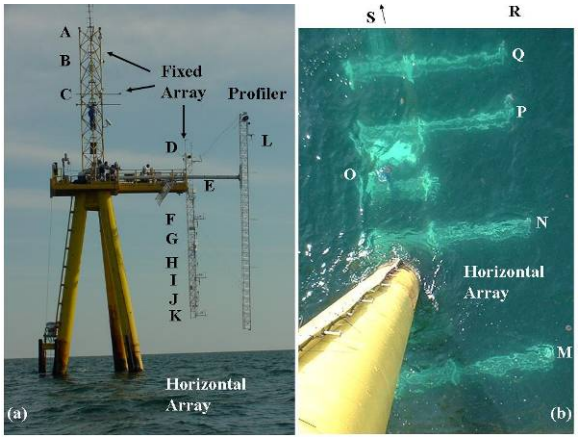


**Figure 6.** a) Experimental setup for the ASIT during CBLAST. The photo indicates the location of the fixed array, profiler, and subsurface horizontal array. b) The subsurface horizontal array photographed from ASIT. The booms extending out from the crossbeam booms support fast response velocity and temperature sensors. The letters are used to reference the location of the instruments that are summarized in Table 1.

Oceanographic sensors were deployed beneath the surface to make similar measurements of currents, temperature, and salinity. Turbulence sensors were mounted on horizontal booms spanning two legs of the ASIT (Fig. 6b) to provide direct estimates of momentum and heat exchange just below the surface. To our knowledge, this represents the first successful attempt to measure directly and simultaneously the heat and momentum exchange on both sides of the air-sea interface. The nominal sampling frequency of the all turbulence and wave instrumentation was 20 Hz.

In addition, a unique Bistatic Coherent Doppler Velocity Profiler (BCDVP) was deployed to provide high-resolution profiles of three component velocity vectors over a 1-m vertical span immediately below the water

surface. The BCDVP was developed by the research group at NPS (Stanton 2001, 2005) and is shown in Fig. 7.

**Figure 7.** The BCDVP being prepared for deployment during CBLAST 2003.

Several acoustic remote sensing devices mounted nearby ASIT on the ocean bottom provided additional velocity measurements. Measurements of horizontal velocity at the sea surface were obtained with a fanbeam ADCP, which produces spatial maps of the surface velocity along four acoustic beams. These measurements produce estimates of Langmuir Cell intensity and scale from patterns of divergence and convergence of the surface velocities (Plueddemann et al., 2001).

Bottom mounted ADCPs near the ASIT and at the nearby MVCO seanode measured vertical profiles of horizontal velocity through the water column. In addition, a 5-beam Broadband Acoustic Doppler Current Profiler (BADCP) was deployed 20-m south of the ASIT in 15-m depth. The 5th, vertically orientated beam of this system directly measures the vertical velocity in a small sample volume, and was used to detect and measure Langmuir cell properties as they advected past the bed-mounted instrument (Elge, 2004).

Surface waves were measured at the ASIT using downward looking laser and microwave altimeters. Directional wave spectra were estimated from the ADCP measurements at the MVCO seanode. The type and location of the fixed sensors on and nearby ASIT are summarized in Table 1.

***Surface mooring array.*** Surface mooring arrays were deployed in the CBLAST-LOW operating area south of Martha's Vineyard during all 3 field campaigns. Two moorings were deployed 20 and 40 km offshore in 2001 to collect records of surface forcing and temporal evolution of vertical ocean structure (Pritchard and Weller, 2005). These records revealed the significant impact of synoptic weather systems on regional oceanographic variability. To resolve this variability and examine the ability of regional atmospheric and ocean models to simulate it, an array of six moorings was deployed from late June to early September 2002 spanning a 20 km wide by 40 km long region south of the Vineyard (Wilkin, 2006).

During the August 2003 IOP, surface meteorological and upper ocean measurements were collected from 15 instrumented surface moorings (Fig. 2). Five "heavy" moorings supported surface meteorological and in the ocean temperature, salinity, and velocity sensors with 2-m vertical resolution. Ten "light" moorings supported temperature sensors with 2-m vertical resolution. The goal was to obtain a continuous 3-D picture of the oceanic temperature field to investigate mesoscale variability in upper ocean dynamics and air-sea coupling.

Three of these heavy moorings supported a full suite of ASIMET instrumentation for air-side measurements. The ASIMET buoys provide heat, freshwater, momentum fluxes using bulk formulae to investigate spatial variability of the fluxes that force/respond to ocean, provide realistic forcing fields to ocean modelers, verify atmospheric model surface meteorological and flux fields, and contrast the closer to shore ASIT and MVCO sites with offshore sites.

***Ship-based surveys.*** Ship-based operations where conducted during all three summers. During the August 2003 IOP surface meteorological and upper ocean measurements were collected by the *F/V Nobska* during four survey cruises. The *Nobska* deployed and tracked 5 drifting buoys each outfitted with a high resolution (0.5m) vertical temperature array and two levels of salinity measurements as shown in Figs. 8 and 9.

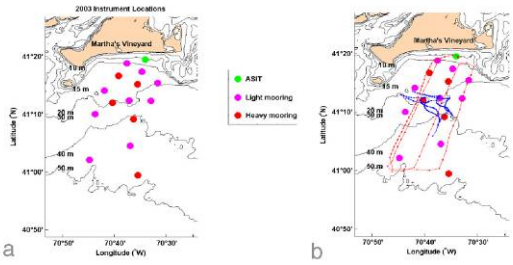


**Figure 8.** Example tracks (blue) from one deployment of the drifting thermistor strings deployed during the IOP and of one deployment of the towed chain by FV Nobska (red) during the IOP to illustrate the additional sampling done over a wide range of spatial scales.

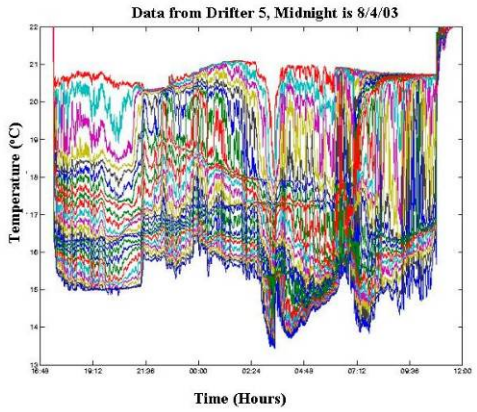


**Figure 9.** Temperature measurement from the T-chain deployed beneath the surface drifters. The upper trace (red line) is from approximately 2.2 m depth. The subsequent lines are at 0.5 m resolution down to the lower trace taken at a depth of approximately 14 m. The measurements collapse during launch and recovery.

The *Nobska* also towed a similar vertical array with fast response temperature or temperature/salinity sensors through targeted surface features and routinely made CTD (conductivity, temperature, depth) profiles. The ship carried upward and downward looking IR radiometers to estimate the sea surface temperature (SST), a direct covariance flux system (DCFS), and shortwave and longwave radiometers to make continuous measurements of the momentum, heat, mass, and radiative fluxes during the oceanic surveys (Fig. 10a).

Surfactant film distributions were surveyed during the 2002 and 2003 IOPS using a new survey tool, SCIMS (Slick Chemical Identification and Measurement System). SCIMS is a semi-autonomous mobile instrument platform deployed off the *R/V Asterias* that detects the presence of surface microlayer films and allows mapping of their spatial and temporal distributions (Fig. 10b). Measurements to characterize surface films were carried out under different wind stress conditions in order to determine the patchiness of surface film distributions on scales ranging from 10 m to 5 km.


**Figure 10.** a) Instrumentation deployed on the Nobska during the 2003 IOP. Bow instrumentation included a direct covariance flux system and IR radiometers. The boom supported an array of temperature/salinity sensors for high-resolution vertical profiles. b) Photo taken from the Air-Sea Interaction Tower at MVCO of the SCIMS catamaran accompanied by R/V Asterias during a southeasterly survey transect on August 15, 2003. Numerous banded surface film features (light areas) evident in the field of view were quantified by SCIMS instrumentation.

***Aircraft Measurements.*** Three aircraft participated in CBLAST-LOW: a Cessna

Skymaster providing IR remote sensing and two aircraft that provided measurements of the mean and turbulent structure of the ABL. NOAA's Long-EZ airplane (N3R) provided measurements of atmospheric turbulence from 10-m to the top of the boundary layer. Its aerodynamic characteristics were well suited for long-duration flights. The aerodynamic configuration of the Long-EZ allows for safe low-speed and low-altitude flight within the constant flux layer.

The Long-EZ relies on differential Global Positioning System (DGPS) technology that allows the measurement of position, velocity and attitude at a 10-Hz sampling rate. The aircraft is instrumented with a suite of various sensors for the measurement of horizontal and vertical wind velocity, pressure, air temperature, humidity, and net (long and short) radiation. Fluxes of heat, moisture, momentum, and trace species can be derived through eddy correlation techniques from the data acquired by this instrument suite.

An automated algorithm is used to identify the averaging time scale for each individual flight segment (and each 1-h record from the tower) that captures the turbulence while reducing contamination by inadvertently captured mesoscale motions (Vickers and Mahrt, 2005). The method is based on identifying the gap region in the multi-resolution heat flux frequency analysis. Once the perturbation quantities are computed based on the variable averaging scale, the fluxes are averaged over a larger window corresponding to 8 km to reduce random sampling errors. Direct covariance fluxes of heat, moisture, and momentum are derived using this approach as described by Vickers et al. (2001). Results from the 2001 IOP are reported by Vickers and Mahrt (2006) and Grimmett et al. (2007).

The CIRPAS Pelican is a similarly instrumented aircraft designed to measure atmospheric turbulence, mean variables, and remotely sensed sea-surface characteristics. The Pelican was used to map atmospheric boundary layer structure in support of the CBLAST-LOW 2003 investigations.

***IR Remote Sensing.*** Measurements of SST variability were made in 2001 from the Long-EZ and in 2002 and 2003 from the Cessna Skymaster. The Skymaster supported a state-of-the-art, high spatial resolution IR imaging system providing calibrated, sky-corrected imagery of SST (Zappa and Jessup, 2005). The system relied on two complementary IR sensors: A longwave infrared imager sensitive to radiation in the 8-12 μm wavelength range that provided high spatial and temporal resolution imagery, and a narrow field-of-view radiometer in the 8-14 μm wavelength range that provide calibrated surface temperature at lower resolution (Fig. 11).


**Figure 11.** The top panel is a picture of Cessna Skymaster chartered for CBLAST-LOW 2002 and 2003. Picture on the bottom left is a close-up of the cargo door on the Cessna Skymaster that was modified to accommodate our downward-looking instruments. Picture on the bottom right is a close-up of the downward-looking infrared imager, collocated video camera, and collocated, narrow FOV infrared radiometer.

For the nominal altitude of 610 m in 2002 and 875 m in 2003, the spatial resolution of the IR imagery was less than 0.3 m and 0.9 m, respectively, compared to 80 m and 115 m for the radiometer. The IR imager operated with a thermal resolution of roughly 20mK that is

an order of magnitude better than that for the IR radiometer. A downward-looking digital video camera was used to supplement these measurements with characterization of the sea surface condition. The surveys in 2002 and 2003 quantified the horizontal variability in the SST field (Fig 12) and investigated links between SST variability, ABL structure, and air-sea fluxes.

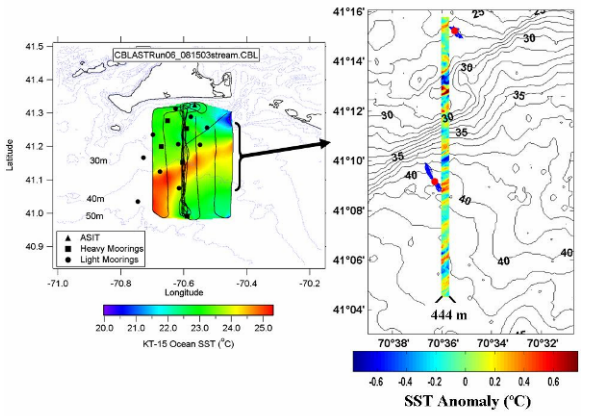


**Figure 12.** Left panel: An illustrative example of the SST maps provided by the IR system overlaid on the bathymetry. These preliminary images were provided to a CBLAST-LOW PI after each run to assist in coordinated ship and aircraft observations. Right panel: An example of the high resolution IR imagery deployed from the Cessna aircraft. The color region represents a 444 m wide swath of SST anomaly relative to a 2.3 km along-track smoothed SST field.

The aircraft efforts were closely coordinated with the ship-based surveys. For example, the thermistor array was routinely towed through features identified during the IR aircraft flights. Additionally, the DCFS fluxes, measured at 8 m, complemented the 30-m flux estimates measured from the CIRPAS Pelican. Analogous to the flux estimates, the radiometer measurements from the *Nobska* complemented the IR aircraft measurements and provide a strong link between these two platforms.

***Nantucket Field Site.*** CBLAST-LOW observations also include extensive measurements from the south coast of Nantucket Island, MA, about 50 km southeast of the CBLAST ASIT tower. Main measurements made from the Nantucket site included rawinsonde launches (Loran-C sondes) every 4-6 hours, turbulence and mean measurements from a flux tower, and continuous sampling of the lower boundary layer from a SODAR. The measurement periods on the Nantucket site were between July 31 and August 23 in 2002 and from July 22 to August 27 in 2003.

During the 2002, the flux tower was comprised of a 10-m mast supporting an infrared hygrometers and sonic anemometer to measure heat, mass and momentum fluxes and associated means In 2003, the 10-m mast was replaced by a 20-m mast and an additional level of turbulence sensors was added. In both 2002 and 2003, a 2-m mast was instrumented next to the main mast to measure air temperature, RH, wind speed and direction, air pressure, precipitation, and downward solar and IR radiation at 1-minute intervals.

The Nantucket instrument suite also includes a Remtech (PA2) SODAR system and a laser ceilometer to measure the cloud base height as well as the backscattering profiles from the aerosol layer near the surface. The SODAR measurement generated mean profiles of the mean wind and vertical velocity at 30-minute intervals with a vertical resolution of approximately 40 m. The measurements also produced the standard deviations of the three wind components, the momentum fluxes of the wind components (u'v' and u'w') and the atmospheric static stability up to the height of 800 m. The total vertical momentum flux, the turbulent kinetic energy (TKE) and the turbulence intensity for the three wind components were also calculated.

**COUPLED MODELS.** One of the main objectives of CBLAST-LOW project is to improve surface and boundary layer parameterizations in Naval Research Laboratory's Coupled Ocean/Atmosphere Mesoscale Prediction System (COAMPS®) for

low-wind conditions. Real-time COAMPS® weather forecasts provided for the CBLAST-LOW field experiment are being used with the measurements to evaluate the model physics and investigate the impacts of air-sea interaction on the mesoscale weather prediction.

The COAMPS® model (Hodur, 1997) has surface fluxes computed using a modified Louis scheme (Louis, 1982) as described by Wang *et al*. (2002). The domain configuration for the real-time atmospheric forecast includes three horizontally nested grids of 27 km, 9 km and 3 km and 30 vertical levels. The SST used in forecasts was assimilated using satellite retrievals and ship observations.

The major improvement to COAMPS includes the reformulation of the transfer coefficients under the convective low-wind regime and the enhanced ability to deal with different momentum and scalar roughness lengths. The modified surface parameterization consistently improves the SST prediction in coupled ocean-atmosphere simulations as demonstrated in Pullen *et al*. (2005).

An example of COAMPS® derived humidity and temperature fields compared against the rawinsondes data for August 2002 is shown in Figs. 13 and 14. The general trend of the forecast agrees well with observations. This includes the drying and cooling trend observed during the first 10 days when low-pressure systems over the continental U.S. frequently interrupted the high-pressure pattern off the east coast region. The southwesterly winds again dominated after 14th of August 2002, providing warm and moist air to the CBLAST area. It is evident that the COAMPS® produced a moister boundary layer (below 1 km) between the 16th and 20th and a cooler boundary layer between the 6th and 10th. The predicted cooler marine boundary layer may be partly attributed to the known near-surface cold bias over land in COAMPS®, which was advected to the CBLAST-LOW area.

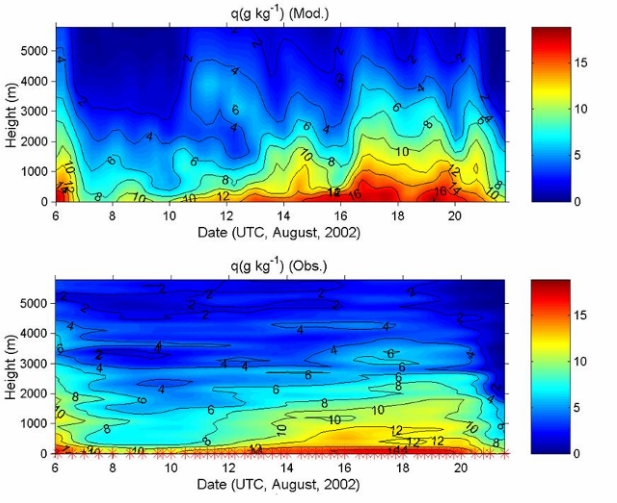


**Figure 13.** Temporal evolution of specific humidity vertical profiles from COAMPS® 3-km grid results (upper panel), and the Nantucket rawinsonde launches (lower panel). The red (*) at the bottom indicates the time of all soundings used to generate the plot.

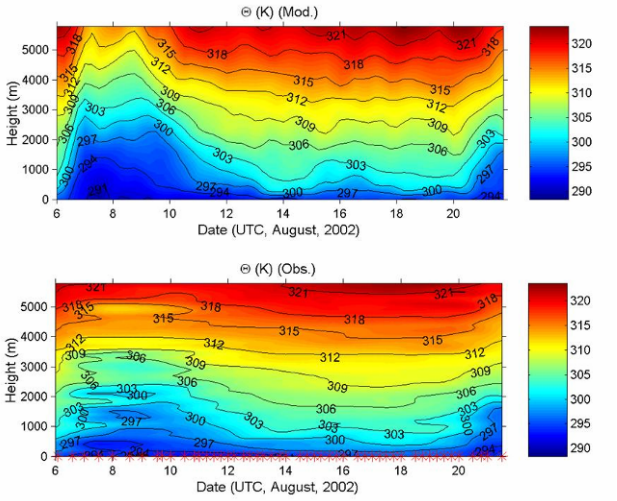


**Figure 14.** Temporal evolution of potential temperature vertical profiles from COAMPS® 3 km grid results (upper panel), and the Nantucket rawinsonde launches (lower panel). The red (*) at the bottom indicates the time of all soundings used to generate the plot.

Another objective of CBLAST was to couple the mesoscale atmospheric model in COAMPS® with the Regional Ocean Modeling System (ROMS). ROMS is a high-resolution hydrodynamic model that has gained wide acceptance in the oceanographic community. ROMS was formulated for the

region using detailed bathymetry. The model is forced by tides, outer shelf climatological inflows, observed downward radiative fluxes, and air-sea heat and momentum fluxes derived from the model SST and COAMPS® forecast atmospheric conditions (Wilkin and Lanerolle, 2005).

The 3-dimensional evolution of regional ocean thermal stratification was simulated successfully, as validated by comparisons to mooring observations (Fig. 15) and satellite imagery (Wilkin, 2006). Tides proved important to the regional circulation, and accurate representation of tidal variability in the model was achieved by assimilation of sea level data to adjust the tidal harmonic forcing open boundary conditions (He and Wilkin, 2006). One role for ROMS is to provide insight into process not resolved observationally. For example, lateral advection and sub-mesoscale mixing of heat are potentially significant in the local heat budget and ROMS was used to gauge the magnitude of horizontal heat transport compared to air-sea heat transfer (Wilkin, 2006).

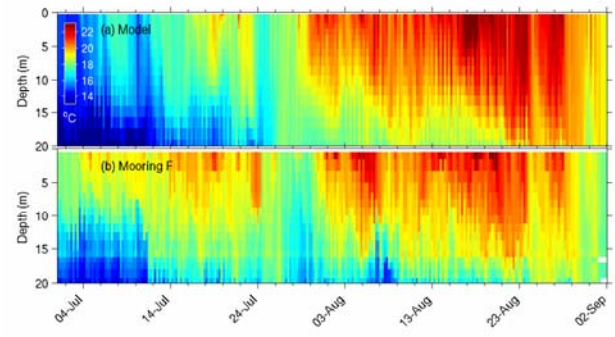


**Figure 15.** Time series of vertical temperature profile at the location indicated by Heavy Mooring F in Figure 2. The upper panel is shows results from ROMS, and the lower panel displays measurements from Heavy Mooring F.

**COUPLED BOUNDARY LAYER PROCESSES.** Marine scientists have long relied on flux-profile relationships that relate the turbulence fluxes of momentum, heat and moisture to their respective profiles of velocity, temperature, and water vapor. These relationships have been investigated in overland experiments since the mid-sixties which and a number of similar semi-empirical functions such as the commonly used Businger-Dyer formulae (Businger, 1988) have been proposed. This approach is reasonably accurate as long as the boundary layer is horizontally homogeneous and the turbulent exchange is driven by a combination of mechanical and buoyant forcing. However, the coastal boundary layers are often characterized by significant mesoscale variability in, e.g., surface temperature and roughness. Additionally, near the ocean surface, wave induced forcing is expected to influence the characteristics of the near surface flow.

Wave-induced effects have been shown to cause substantial departure from land-based parameterizations (e.g., Vickers and Mahrt, 1999; Smedman et al., 1999; and Hare et al. 1997) in the wave boundary layers (WBLs). The WBLs are defined in this overview as the region where the total momentum flux, even if assumed to be constant with height, has a significant wave-induced component (e.g., Hristov et al., 2003). Since land-based parameterizations are formulated for turbulently driven processes (i.e., wind shear and buoyancy), they become increasingly inaccurate in the WBL as one nears the surface. This applies to both the atmospheric and ocean boundary layers. For example, coherent structures in the mixed layer, known as Langmuir circulations, are driven by wave-current interactions. These structures are believed to transport buoyancy and momentum and enhance mixing. Additionally, intermittent turbulence and additional mixing is generated by wave-breaking. Neither of these processes is generally included in flux-profile relations, which implies that these processes are not accounted for in most models.

CBLAST-LOW data analysis and modeling efforts are directed towards improved understanding of how mesoscale variability and wave-related processes affect the coupled boundary layer. Many of the investigations in CBLAST-LOW have relied on large eddy simulations (LES) and direct numerical simulations (DNS) to guide the observational process studies as summarized in Table 2. The numerical results provide a context for interpreting our measurements and investigating resolved processes, while our measurements have provided a means to evaluate sub-grid-scale parameterizations required by the models. For example, in the process studies described below, LES is used to guide investigations of wind-swell interaction, and the impact of SST variability on the coupled boundary layers.

***Momentum Exchange Above the Air-Sea Interface.*** The bulk aerodynamic formulae parameterize the sensible heat, latent heat, and momentum fluxes in terms of the more easily measured mean or bulk quantities using transfer coefficients. The transfer coefficient for momentum, i.e., the drag coefficient, computed from the CBLAST-LOW data set show good agreement in the mean with the COARE 3.0 algorithm (Fairall et al., 2003), particularly between 4 and 12 m/s as shown in Fig. 16. However, there is significant disagreement between the bin-average data and the parameterization at the lowest and highest wind speeds.

We hypothesize that the larger values of the drag coefficient at high winds speeds is likely due to shoaling waves that produce steeper waves and enhanced breaking. Preliminary indications are that a number of physical processes driven by wind-wave interaction are responsible for the disagreement at low wind speeds. For example, for conditions with weak wind following faster moving swell, the wind stress may be reduced relative to the bulk prediction. These conditions are known as old seas and are commonly found over the ocean whenever non-locally generated waves propagate into a low-wind region or whenever local seas slowly decay as a storm moves out of the region.

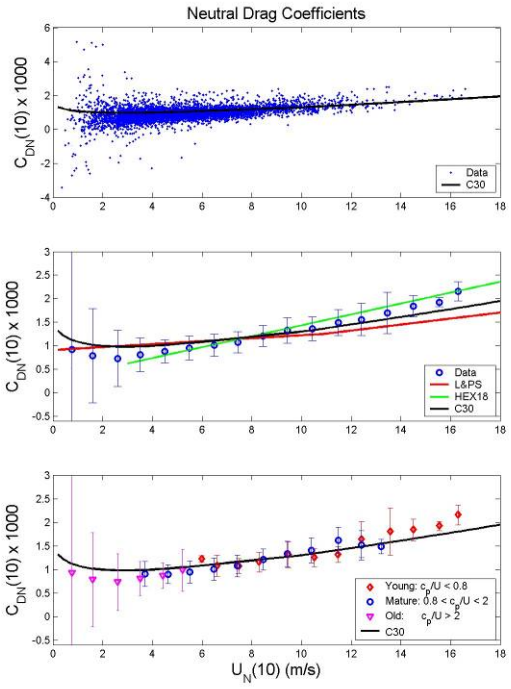


**Figure 16.** Individual (top panel) and bin-averaged (middle and lower panel) estimates of the neutral drag coefficient. The black lines labeled with C30 represent the COARE 3.0 parameterization from Fairall et al. (2003). The bin-average estimates in the middle panel are also compared with an average parameterization derived from Large and Pond (1981) and Smith (1980) denoted by L&PS, and the HEXOS parameterization given by Smith et al. (1992) denoted by HEX18. L&PS and C30 were developed using open ocean data sets, while HEX18 was developed from data taken in coastal waters where the water depth was 18-m. The lower panel provides bin-average results for subsets of the data that were measured in young, mature and old seas as characterized by the wave age parameter $c_p/U$.

The sea-state can be characterized by the wave age parameter $c_p/U$, where $c_p$ is the phase speed of the dominant waves and U is the wind speed. The wave-age of a mature (fully developed) sea is approximately 1.2, implying that the wind and waves are moving at approximately the same speed. The wave-age of younger seas fall below this value (i.e., developing or depth limited waves where the

wind speed is greater than the phase speed), while wave-ages for older (decaying) seas fall above this value.

The lowest panel of Figure 16 plots the bin-averaged results for three subsets of the data that were measured in young, mature and old sea. The drag coefficients for a range of wave ages ($0.8 < c_p/U < 2$) that includes mature seas are in good agreement with the COARE parameterization, which was developed using open ocean observations. If the COARE parameterization is correct for mature seas at all wind speeds, then the bin-averaged results indicate that the drag coefficients of the younger seas are enhanced while those of the older seas are suppressed. Additionally, the drag coefficients of younger seas agree reasonable well with the formulation developed by Smith et al. (1992) during the HEXOS experiment, which was conducted at a similar water depth.

The figure also shows, however, that the difference between the drag coefficients for wind speed bins that have more than one wave-age category is not significant. Therefore, these results, by themselves, are not sufficient to conclude that wave-age is the cause for the discrepancy (i.e., COARE may simply overestimate the drag at low wind speeds for all wave-ages). Nonetheless, we have reason to believe that swell impacts air-sea exchange at low winds based on previous field results (e.g., Smedman et al., 1999) and numerical simulations conducted for CBLAST. For example, our recent investigations of wind-swell interaction at low winds have been guided by LES studies by Sullivan et al. (2004), which clearly show that fast moving swell in light winds can have a significant effect on the wind field up to heights of O(100m) as shown in Fig. 17.

The LES results indicate that the dominant forces above the waves in this region are a wave-induced momentum flux divergence that accelerates the flow and a retarding pressure gradient, i.e., opposite to the momentum balance in classical boundary layers. Under these conditions, the wave driven winds produce a low-level jet and a rapid decay of the momentum flux with height (Sullivan et al., 2004). We have begun to investigate these processes using the ASIT data to examine the vertical structure of the turbulence in the surface layer, looking at how well the traditional predictions of the wind profiles compare with measurements over growing (young), fully developed (mature), and decaying (old) seas.

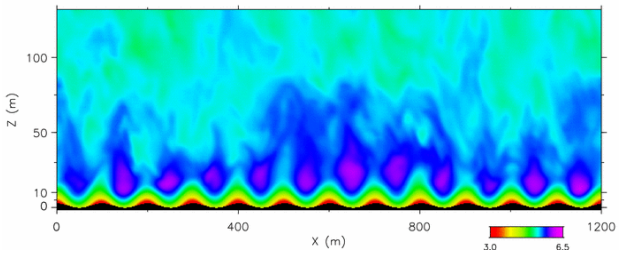


**Figure 17.** An LES snapshot of the instantaneous horizontal winds in a neutrally stratified boundary layer with mean 10-m wind speed of 5 m/s and a wave age of cp/U of 2.2. The color bar indicates the range of winds speeds 3.0 and 6.5 m/s. The wave height and wavelength are set to 1.6 m and 100 m, respectively. Maximum wind speeds denoted by purple shading are found at a height of approximately 20-m.

***Momentum Exchange Beneath the Air-Sea Interface:*** The vast majority of the flux parameterizations for the oceanic surface boundary layer can be traced back to the atmospheric community. Since the actual ocean-side fluxes have never been reliably observed (i.e. from direct covariance measurements), attempts to validate these parameterizations have been indirect. Therefore, a primary object of the oceanographic component is to evaluate flux parameterizations (e.g. eddy diffusivity and eddy viscosity) based on direct measurements of the momentum flux and associate shear, and heat flux and associated temperature gradient that characterize the near subsurface ocean from the crest-trough region of surface gravity waves to the base of the mixed layer.

A second goal is to determine the oceanic processes that support the fluxes and transfer the momentum and heat further down into the water column. Near the surface, shear stress and energetic bursts of turbulent energy injected into the water column by nearly continuous micro-breaking and more episodic whitecap breaking waves are believed to transfer momentum and heat from the surface into the mixed layer. The momentum and heat are then transferred through the mixed layer by turbulent eddies and other processes.

The subsurface array of turbulence sensors on ASIT (Fig. 6b) was used to directly measure heat and momentum fluxes. The oceanic momentum fluxes were estimated by direct covariance at 1.7 and 2.2 m depths and checked against an independent method that relied on the airside measurements. The direct covariance estimates were made by integrating u'w' cospectra (where u' is the horizontal and w' the vertical velocity fluctuations, respectively) from zero up to an adaptive cutoff frequency below the wave band. This allowed estimation of the stresses carried in eddies approximately 1 m and larger. The independent estimates were made by assuming a slab-like mixed layer and interpolating between the measured wind stress at the surface and zero at the mixed layer base.

These estimates of stress match well at low wind speeds (Fig. 18), suggesting that all the stress at 1.7 and 2.2 m depths is carried in eddies larger than ~1 m. Stress being carried by large eddies is consistent with the predictions of Kaimal et al. (1972) for turbulence generated by shear and convective instabilities. It is also consistent with observed sizes of coherent structures known as Langmuir circulations (Plueddemann et al., 1996).

These investigations are aided by an acoustic device know as the BDCVP. The BCDVP provided 1-cm resolution profiles of three component velocity vectors and backscatter levels over a 1-m vertical span immediately below the water surface under limited fetch wind waves. The continuous, dense profile of velocity vectors have allowed Reynolds stresses to be estimated through the water column in a surface-following coordinate system. The BDCVP was deployed for 6 days under limited fetch wind waves with winds ranging from 3 to 10 $ms^{-1}$. This has provided a unique data set to investigate the transfer of momentum under waves (Stanton, 2004).

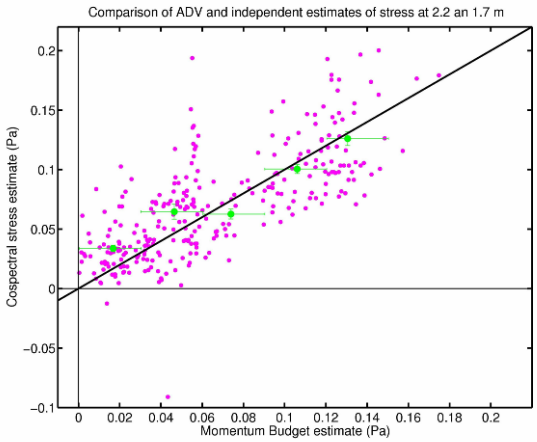


**Figure 18.** Cospectral estimates of momentum flux measured at 1.7 and 2.2 m depths versus an independent estimate from a momentum budget based on air-side flux estimates. Small pink dots are individual burst measurements. Larger green dots are bin averages formed by binning in 0.02 Pa increments along the horizontal axis. Vertical error bars denote two standard errors of the scattered observations about the bin average value. Horizontal bars show the extent of the bin from which each average was computed.

A 100 second timeseries of the BCDV observations during local wave breaking events in Fig. 19 shows the entrainment of air-bubbles into the water column by coherent vertical structures deeper in the water column. Here, the acoustic backscatter and velocity fields have been mapped into a surface-following coordinate system. The larger data set is being analyzed to parameterize the stress imparted by the breaking waves and the long-lived coherent Langmuir Circulation cells described in the following section.

***Langmuir Circulation.*** A leading candidate for rapid heat and momentum transfer through

the surface mixed layer is coherent circulation structures known as Langmuir circulation (LC). The fluxes associated with LC have been inferred, but never measured. Attempts to parameterize LC mixing in 1-D ML models are in their infancy. If the dominant process supporting near-surface fluxes is strongly tied to the wave field, then most existing models (which rely on wind and buoyancy forcing only) are not capturing all of the necessary physics.

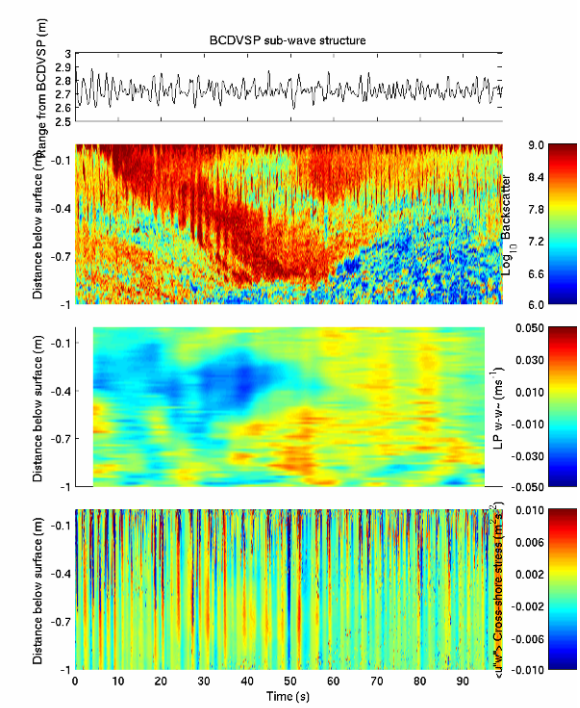


**Figure 19.** A 100 second profile timeseries of a.) surface elevation, b.) acoustic backscatter levels, c.) low pass filtered vertical velocity and d.) u'w' stress component correlations measured under short period, limited fetch wind waves. Bubbles injected during a wave breaking event at t=7 seconds were entrained by a sub-surface circulation cell seen in the vertical velocity profiles that have the wave-period motions filtered out.

The coastal setting of CBLAST provided more variability in the observed sea states than typically found over the open ocean due to variable fetch and water depth. For example, at a given wind speed, the air-sea momentum flux in growing seas may be significantly larger than that in fully-developed seas. Wave spectrum in growing seas is narrowly peaked so that the Stokes drift current will be different. Secondly, the presence of a frictional bed generates a bottom boundary layer that interacts with the surface boundary layer in shallow water. LES simulations have been conducted at the ocean surface layer under a wide range of wind and wave conditions to investigate how the turbulence characteristics change with the sea state.

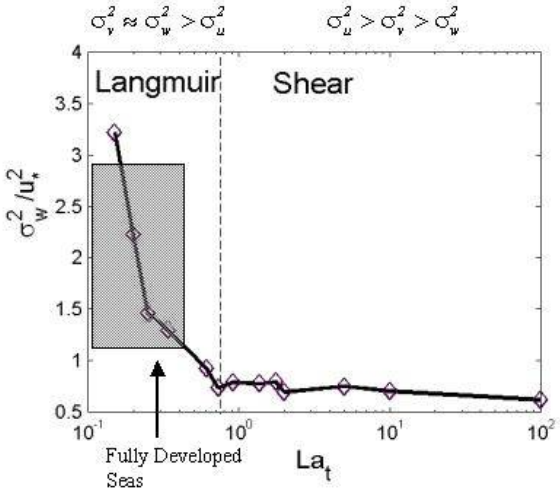


**Figure 20.** The depth-averaged vertical velocity variance normalized by the friction velocity as a function of $La_t = u_*/U_s$ where $U_s$ is the Stokes drift. The shaded grey box indicates the range of vertical velocity variances observed in the upper ocean over deep water while a fully-developed sea corresponds to $La_t$ =0.3 (from Li et al., 2005).

Li et al. (2005) constructed a regime diagram to differentiate buoyant-, shear- and wave-driven turbulence in the ocean surface layer. All three types of turbulent flows are anisotropic but show different orderings of turbulence intensities. In the absence of buoyancy/stratification, turbulence in the wind-driven upper ocean shows a transition from Langmuir to shear turbulence as the turbulent Langmuir number (ratio of friction velocity to surface Stokes drift) increases (Fig. 20).

A fully-developed sea state corresponds to $La_t \approx 0.3$ and lies within the Langmuir regime. When $La_t$ is greater than 0.7, the normalized vertical turbulence intensity increases rapidly with decreasing $La_t$ due to additionally turbulence generation due to

Stokes drift. Vertical turbulence intensity in Langmuir turbulence is about two times larger than that in shear turbulence and falls into the range observed in the upper ocean over deep water (D'Asaro, 2001; D'Asaro & Dairiki, 1997). In fetch-limited conditions over shallow water, however, $La_t$ is expected to increase into the shear regime. When $La_t$ is greater than 0.7, the ratio is nearly constant, indicating that the turbulent intensity can be scaled by the friction velocity only as expected in shear turbulence.

Several of the velocity sensors were deployed for the specific purpose of investigating LC mixing. Measurements of water velocity at the sea surface from the fanbeam ADCP show patterns of convergence and divergence at scales of a few tens of meters (Fig. 21), which can be used to identify Langmuir circulation (LC). When winds are moderate and waves are small or decaying, LC is typically poorly developed as shown by the left panel in Fig. 21. However, the right panel shows that LC is clearly distinguishable under similar wind speeds when the wave field is growing.

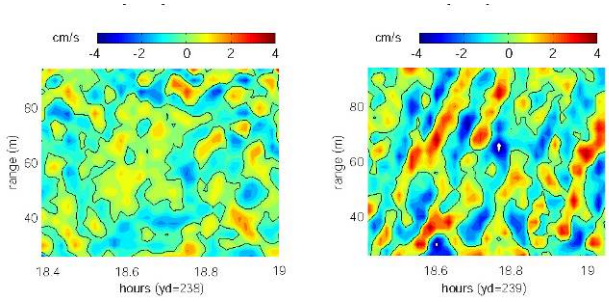


**Figure 21.** Time-range plots ow water velocity at the sea surface based on fanbeam ADCP measurements during CBLAST-LOW.

Modulation of LC strength during CBLAST-Low appears to be strongly related to wind direction, emphasizing the role of limited fetch (e.g. winds from the W, N and NE are fully or partially blocked by the island of Martha's Vineyard, whereas winds from the south produce well-developed seas). Future work will examine the relationship of LC strength to surface forcing by wind and waves, with particular attention to the influence of the wave age parameter $C_p$ / $u_*$, where $C_p$ is the phase speed of the locally-forced wind waves and $u_*$ is the oceanic friction velocity. Partitioning of the wave spectrum into forced wind-waves, decaying wind waves and swell will be a key aspect of the study.

The Broadband Acoustic Doppler Current Profiler (BADCP) was deployed 20 m south of the ASIT in 15-m depth. This instrument recorded the velocity field spanning the water column for three months during the fall of 2003. Continuous 0.5 Hz sampled velocity profiles were measured with 0.5-m vertical bins from 1-m above the bed to the ocean surface under winds ranging from 1 $ms^{-1}$ to 18 $ms^{-1}$. The fifth, vertically orientated beam of this system directly measures the vertical velocity in a small sample volumes through to the surface that are being used to detect and measure Langmuir cell properties as they advected past the bed-mounted instrument (Elge 2004).

The extensive time-series from the BADCP, fanbeam ADCP and other ASIT observations, and being combine with LES and high resolution coastal ocean models to develop parameterizations for sub-grid scale processes like the transfer of stress through Langmuir circulations. Comparisons of the intensity of cross-wind, downwind and vertical motions for different wave age and wave heights are being made with LES model predictions made by Li et al 2005. Further LES model runs of wind and tidally forced coastal areas representing selected ASIT observations are being considered.

Ultimately, development of mixed layer parameterizations including LC mixing and improve capability to simulate their effect in ocean models. For example, short-term (e.g. 24-72 hr) prediction of mixed layer properties (e.g. SST and near surface currents) with standard mixed-layer models has been shown

to fail when the "flywheel effect" of LC mixing is important (e.g. for decaying wind seas; Plueddemann and Weller, 1999). Modifying the mixing parameterization to include properties of both the wind and wave field would be expected to solve this problem.

***DNS of Near-Surface Processes***. A collaborative effort between the research groups at MIT and JHU have developed direct simulation (DNS) capabilities for the atmosphere-ocean-wave coupled flows at small spatial scales. The availability of the instantaneous, three dimensional flow field obtained from simulations provides detailed flow structures and identification of key transport processes in the atmosphere-ocean wave boundary layer. In the simulations, both the air and water turbulent flows are solved simultaneously in order for the coupling dynamics to be captured.

At the air-water interface, fully-nonlinear free-surface coupled boundary conditions are used, with the kinematic boundary condition requiring that the interface remains a material surface, and the dynamic boundary conditions requiring a stress balance across the interface. Two novel and complementary computational approaches are used: (i) at low wind speeds where the surface waves are of small magnitudes, a boundary interface tracking method utilizing boundary-fitted computational grids; and (ii) as the wind speed increases and the waves steepen and break, an Eulerian interface capturing method based on a level set approach.

One important discovery from these simulations using the first approach is yet another mechanism to drive airside low-level jets very close to the interface. Similar to the low-level jets found in our LES, these micro-jets are induced by the water motions underneath. In this case, however, the water motion is the representative of the small vortices driven by micro-breaking at the air-sea interface. A typical example is shown in Fig. 22, which plots the conditionally averaged results of quasi-streamwise vortices. The negative streamwise vortex in the water induces a positive mirror vortex in the air above.

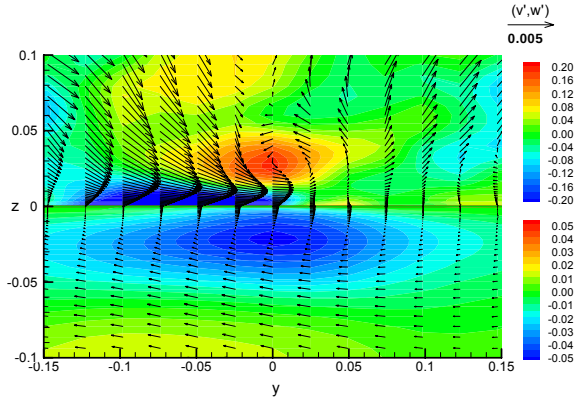


**Figure 22.** Quasi-streamwise vortex on the waterside ($z < 0$) and the induced mirror vortex and micro low-level jet on the airside ($z > 0$). Shown in the figure are contours of streamwise vorticity component $\omega_x$ and fluctuation velocity vectors ($v'$, $w'$ )on a vertical ($y$, $z$) cross-section which is located at the center of the quasi-streamwise vortex. Plotted are conditionally-averaged results based on about 3000 instantaneous quasi-streamwise vortices.

It is interesting that a micro low-level jet is formed on the airside between the induced mirror vortex and the interface. This can be explained by the continuity condition at the interface and by the disparate physical properties of air and water. As water is moved by the waterside quasi-streamwise vortex, diverging and converging flow is induced at the interface. Due to the continuity of velocity at the interface, diverging-converging flow must also present on the airside. Because the shear stress across the interface needs to be balanced and because the value of dynamic viscosity of air is substantially smaller than that of water, velocity gradient on the airside is much larger than that on the waterside. As a result, a jet flow is formed on the airside in the vicinity of the interface.

***Simulations of Mesoscale Variability***. In planning the CBLAST mooring arrays, it was recognized that all spatial scales could be

captured all of the time of interest and would have to rely on numerical models to fill in the details. For example, lateral advection and sub-mesoscale mixing of heat was largely unobserved by the CBLAST-LOW network, yet these processes are potentially significant in the local heat budget. ROMS was therefore used to gauge the magnitude of horizontal heat transport compared to air-sea heat transfer

ROMS has been configured with a high level of realism in order to examine the mesoscale response of inner shelf waters in this region to tides, local synoptic meteorology, and shelf-wide external forcing, and to provide support for the interpretation of CBLAST-LOW mooring observations. The modeling objective is to capture the essential features of the 3-D ocean heat transport on diurnal to several day time-scales, and spatial scales of order 1 km. Furthermore, under low wind conditions during summer heating, the oceanic mixed layer is often only a few meters thick and mesoscale oceanic circulation can potentially modulate the shallow mixed layer depth, thereby affecting sea surface temperature and air-sea fluxes. It is therefore important to consider the vertical flux observations within a regional spatial context of mesoscale variability.

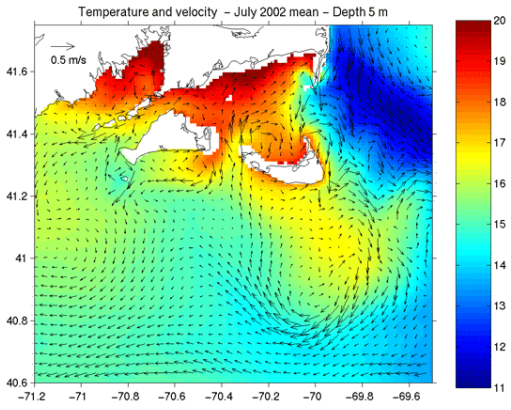


**Figure 23.** Mean temperature and velocity determined by ROMS at 5-m depth.

Over the Nantucket Shoals tides vertically mix the water column, maintaining low SST throughout the summer as shown in Fig. 23. The net downward heat flux into the ocean is exported laterally across a persistent tidal mixing front, and an anti-cyclonic tidal residual flow encircles the Shoals transporting cool waters toward the mid shelf south of MVCO. These cooled waters warm under the influence of surface heating with little depth-integrated lateral divergence, i.e. an essentially one-dimensional vertical heat balance.

Closer to MVCO, near the innermost moorings deployed in 2002 and 2003, only about half the net downward heat flux during July and August goes to warming the water column and establishing strong thermal stratification, while half is removed by horizontal transport. Separating this horizontal heat divergence into mean and eddy contributions, it was found that though the monthly mean circulation cools the water column, a strong tidal eddy heat flux significantly warms the parts of the region.

Tidal phase eddies are generated regularly by the flood tide exiting Nantucket Sound through Muskeget Channel and these eddies carry warm water south and west toward MVCO. The subsequent ebb tide tends to draw cooler water from south of Nantucket back in to the Sound, leading to a net eddy heat divergence that warms the region around MVCO and Mooring F. The modeling study indicates that horizontal advection and mixing of heat must be acknowledged as potentially significant contributors when endeavoring to close the net water column heat budget at individual locations in the CBLAST region.

***Mesoscale Modulation of Air-Sea Exchange.*** The sensible heat exchange driven by differences between the air and sea surface temperatures is a fundamental oceanic forcing of the atmosphere. The exchange impacts atmospheric forcing of the ocean through changes in stratification. SST during CBLAST-LOW had significant short-term temporal (e.g., diurnal) and small-scale (e.g.,

5-10 km) spatial variability, which may have important impact on the atmosphere mesoscale forecast. Coordinated efforts during CBLAST-LOW were designed to observe and identify the processes that spatially modulate the vertical structure of the upper ocean that, in turn, can modulate the air-sea exchanges that couple the boundary layers over a wide range of horizontal scales.

An illustrative example of coupled boundary layer dynamics, as well as of the coordinated observations made during CBLAST, is provided in Fig. 24. The oceanic temperature structure is highly resolved by the thermistor string towed from the *Nobska*. It shows the vertical structure beneath warm, cool and warmer pools as seem from satellite imagery from north to south. The atmospheric structure is not as well resolved due to limitations of aircraft sampling.

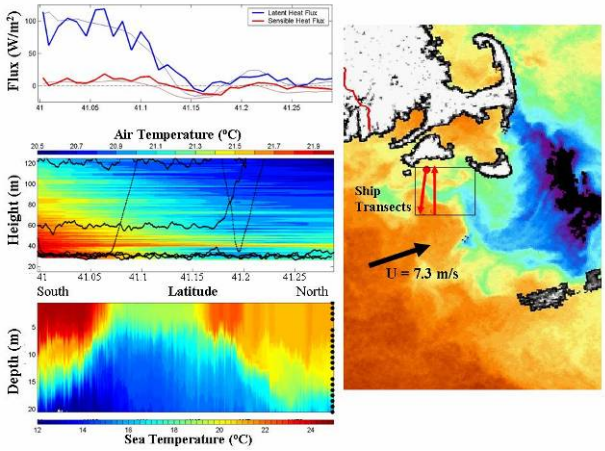


**Figure 24.** On the left, ocean temperature structure (lower), atmospheric temperature structure from the Pelican aircraft (middle), and sensible and latent surface heat fluxes (upper). The depths of the oceanic temperature sensors are indicated by the black dots in the lower panel. The location of the aircraft during low, mid, and upper level flux runs, as well as sawtooth soundings is shown by the black line in the middle plot. The transects were conducted by the FV Nobska on the afternoon of August 19, 2003 as shown on the right. The fluxes were measured during the first transect when the Nobska was steaming into the wind as shown. The oceanic temperature measurements are from the second transect when the aircraft was overhead. The response of the atmospheric boundary layer to the SST field is evident, but the strong spatial variation of heat fluxes also affects the subsequent evolution of the SST field.

However, the measurements clearly indicate a cooling of the near surface over the cool water, and give some indication of warming over the warm water to the north. The surface fluxes are clearly responding to the spatial variability in the SST field. Dramatic change was seen in both latent and sensible heat fluxes (nearly 150 W/m$^2$ total) as the vessel moved across the narrow oceanic frontal zone. However, there also appears to be a lag in the response over the warm water found downwind of the cool tongue. Snapshots like these over the course of the day show diurnal warming over the entire regions. The rate at which sub-regions warm and the corresponding response of the mixed layer will depend on the magnitude of the surface fluxes "locked" over these sub-regions.

***Simulations of Atmospheric Response to SST Variability.*** LES of SST variability was conducted to guide investigations of the effect of mesoscale SST variability on surface fluxes and the marine boundary layer structure (Skyllingstad et al. 2006). The basic scenario for the LES shown is to divide the simulation into regions of alternative warm/cold SST anomaly. Ambient air temperatures upstream and downstream of the anomaly region are set equal to the SST values in Zone 1 and 4, respectively. This creates a neutrally stratified boundary layer upstream of the anomaly region. The boundary layer adjusts to neutral downstream from the anomaly region.

Simulations show that the spatial order, relative to the flow, of warm and cold anomalies has a direct impact on both the boundary-layer structure and the surface fluxes over this downstream region. For example, when the warm anomaly (Zone 2) is upstream from the cold anomaly (Zone 3) the downstream boundary layer exhibits a complex structure because of enhanced convective forcing and mixed layer deepening upstream from the cold anomaly. An internal boundary layer forms over the cold anomaly

in this case, generating two distinct layers over the downstream region (Zone 4) as shown in Fig. 25.

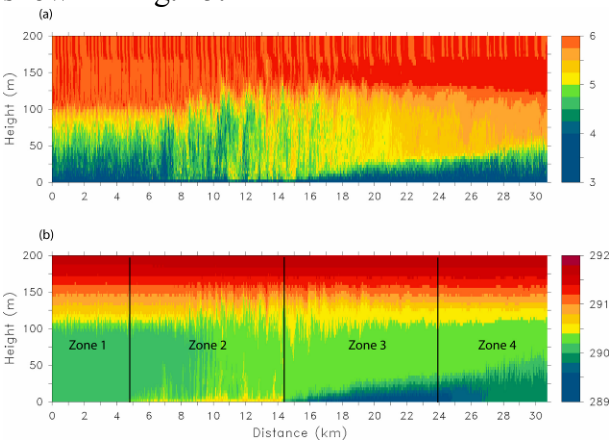


**Figure 25.** Cross section plots in the vertical and horizontal direction showing (a) horizontal velocity (m $s^{-1}$), and (b) potential temperature ($^{o}$C). Surface temperatures are 18 $^{o}$C in Zone 1, 20 $^{o}$C in Zone 2, 16 $^{o}$C in Zone 3, and 18 $^{o}$C in Zone 4, and the wind is from the left. The simulations indicate that the response of the atmospheric boundary layer to these small-scale SST variations would be difficult to parameterize because the boundary layer response depends on whether flow is from warm to cold water or vice-versa.

These results suggest that, for SST differences of 2-4 $^{o}$C and mean wind speeds of 5-10 m $s^{-1}$, SST variability on scales of 5-20 km should be directly simulated in mesoscale models. Parameterization of surface fluxes and boundary layer structure at these scales will be very difficult because of their dependence on sub-grid scale SST variability. However, simulations of similar flow over smaller scale fronts (< 5 km) indicate that small-scale SST variability might be represented in mesoscale models by relating the effective heat flux to the strength of SST variance.

***Processes Responsible for SST Variability: Internal Waves.*** A number of additional field operations aboard the *FV Nobska* were coordinated with those of the CIRPAS Pelican aircraft and the Cessna Skymaster IR imaging aircraft in investigate the processes responsible for SST variability. Conditions in the region on Aug 15, 2003 were ideal for conducting a case study of enhanced SST variability in low winds. Winds were low-to-moderate throughout the day, with wind speeds of 2.5-4.5 m/s in the early morning hours decreasing to speeds of 1-2 m/s by about noon local time.

Nearly overlapping ship transects were carried out, one around 7:30 and another around 16:30 (local time). The mean wind speeds and surface turbulent heat fluxes were similar during the two transects, but the low winds and strong daytime heating led to the development of very strong, shallow temperature stratification, with a temperature gradient of about 2ºC over the upper 2 m.

During the afternoon survey, the shipboard infrared SST measurements indicated that the 10-2000-m SST variability was much larger than it had been in during the morning survey. Ship and aircraft teams, communicating by radio, then devised a strategy to optimally utilize the ship, aircraft, and moorings to better characterize and understand this low-wind SST variability through simultaneous, overlapping surveys as shown in Fig. 26.

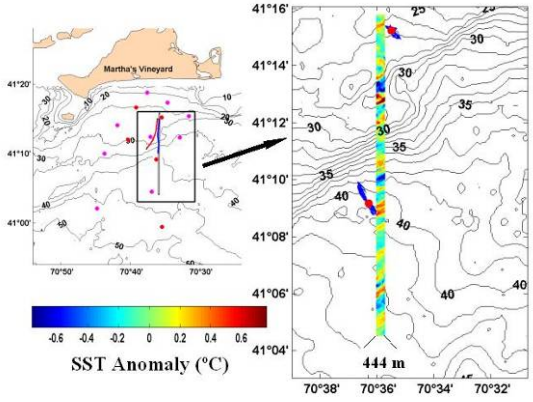


**Figure 26.** Left panel: Diagram showing the 2003 mooring array, the morning ship transect (blue line), the afternoon ship transect (red line), and the aircraft track (grey line) from August 15, 2003. Red and pink dots indicate moorings. Right panel: SST anomaly (°C, colored) relative to 2.3 km along-track, smoothed SST and the current vectors (blue arrows) associated with 30 min. period internal waves at two nearby moorings during the hour centered around the aircraft overpass.

The internal wave crests are expected to be oriented perpendicular to the axis of the wave velocity fluctuations.

Analysis of this case study has proven fruitful; it provides direct evidence that the 100-2000-m SST variability observed under low winds is associated with oceanic internal waves. One piece of evidence for this comes from analysis of nearly coincident airborne SST measurements and mooring data. The mooring data indicated the presence of quasi-linear, energetic internal waves with a period of about 30 minutes during the time of the aircraft overpass. For such high frequency internal waves, the earth's rotation can be neglected, so the horizontal velocity signal of the wave is expected to be rectilinear and normal to the wave crests (i.e. down the pressure gradient). The 20-60 minute band-passed velocity vectors are roughly rectilinear and normal to the crests and troughs seen in the SST imagery (Fig. 26).

More direct evidence of an SST signature of internal waves comes from the coincident radiometric SST and subsurface temperature measurements from the *FV Nobska*. Figure 27 shows the temperature anomaly, relative to the 150-m along-track smoothed temperature, collected from the *FV Nobska* during this period. Data from both the towed instrument chain and the shipboard radiometers are included, and the measurements at nine depths in the upper 5-m of the ocean show that there is a strong vertical coherence of horizontal temperature fluctuations extending from depth to the sea surface.

A similar relationship between surface and subsurface temperature fluctuations exists at a wide range of scales, up to the O(1 km) scales that have been examined to date. The analysis indicates that these spatial fluctuations in SST are associated with oceanic internal waves, which cause temperature fluctuations extending from depth to very near the surface because of the relatively strong stratification that exists throughout the water column under low wind conditions (Farrar *et al.*, 2004a).

However, it is still unclear how the subsurface temperature signal is imprinted on the sea surface. In the simplest of internal-wave models (linear, inviscid, and adiabatic dynamics), internal waves do not have an SST expression, even when a strong near-surface temperature gradient is present. Consistent with the inferences of Walsh *et al.* (1998) and Marmorino *et al.* (2004), this case study provided direct evidence that the SST spatial fluctuations are a surface expression of oceanic internal waves. However, Walsh *et al.* (1998) hypothesized that the SST signal was caused by internal wave modulation of near surface mixing, and Marmorino *et al.* (2004) hypothesized that the SST signal was a result of vertical straining of the cool skin by the internal waves. (The cool skin, or aqueous thermal boundary layer, is an O(1 mm) thick conductive boundary layer that is typically cooler than the bulk fluid because of sensible, latent, and long-wave heat loss from the sea surface.)

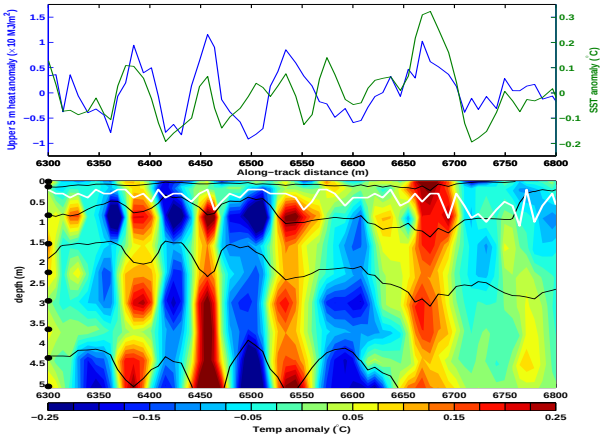


**Figure 27.** Surface (green, upper panel) and subsurface temperature anomaly (lower panel) and upper 5 m heat content anomaly (upper panel, blue line) relative to the 150 m along-track smoothed values. The measurement depths are indicated by black dots on the left side of the figure, and isotherms (black lines) are marked at intervals of 1ºC. The white line marks the depth where the temperature is 1ºC less than the surface temperature.

Both hypotheses take the signal to be due to a fundamental boundary layer process, the former hypothesis being associated with mixing in the turbulent boundary layer and the

latter hypothesis being associated with modulation of the thickness of the aqueous thermal boundary layer. Because of the extremely strong near surface stratification that develops under low winds and strong insolation, the internal waves cause temperature perturbations that extend very near the surface, and either or both hypotheses may be correct. Analysis is proceeding under the hypothesis that the surface signal is due to some combination of near surface mixing, which may directly imprint the signal on the surface, and the surface vertical strain associated with the waves, which may modify the magnitude of the cool skin effect (Osborne, 1965; Marmorino *et al.*, 2004).

***SSR Variability.*** Numerous banded surface film features were also evident on August 15, 2003 as seen in Fig. 7b. While surface films, surfactants, may be the cause of these bands, the visible signature is actually produced by differences in the way that light is reflected off smooth and rougher surfaces. At low winds, subsurface flows often appear to be the dominant process controlling surface film distributions and thereby sea surface roughness (SSR). The 1-Hz record of CDOM fluorescence during this transect is shown in Fig. 28 as ΔCDOM, the difference between the CDOM fluorescence in the microlayer and at 10-cm depth. The record shows strong surfactant banding on different spatial scales. Given a SCIMS catamaran forward speed of 0.5 m/s, the fine scale features are estimated to be ~15-20 m wide, while major bands are up to 200 m in width. Surface film records will be compared with airborne IR imagery, as well as with the fan beam ADCP and temperature data from the buoy array at ASIT to continue the investigations of cause and effect of these slicks and their impact on air-sea exchange.

***Processes Responsible for SST Variability: Coherent Structures.*** Not only have regional variability been observed and related to internal waves, but small-scale structures within the IR imagery that suggest mechanisms that drive or enhance exchange under low wind speed conditions have been observed (Zappa and Jessup, 2005). In particular, extensive regions ($O$(1 km)) with embedded sharp coherent temperature ramps of $O$(0.5ºC) with spacing of $O$(10 m) during moderate winds (2.5 to 5 $ms^{-1}$) as shown in Fig. 29 have been observed.

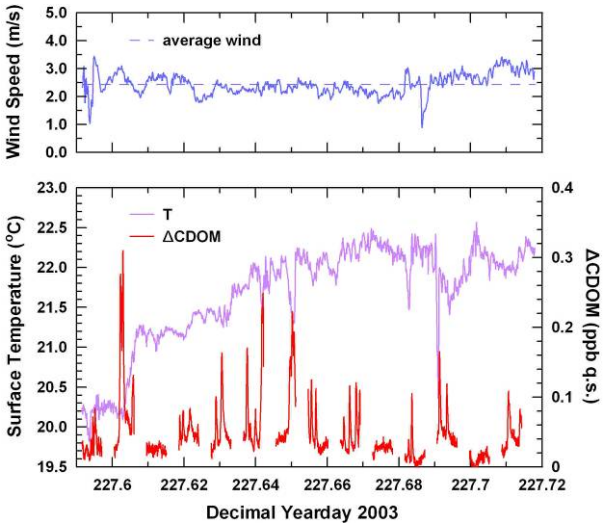


**Figure 28.** Lower panel: ΔCDOM and surface temperature records for Yearday 227, 2003 showing correspondence between surface temperature anomalies and surface chemical enrichments. Upper panel: Wind speed for the same transect.

These coherent ramp structures may be the IR signature of a mechanism in the near-surface layer that leads to the stratification breakdown as the wind-driven shear erodes the near-surface stratification that was established during the peak daytime heating. The dominant spatial scale of the variability in temperature across these coherent ramps is 14.7 m, and they extend over several km. The lack of coherent parallel features in the visible imagery suggests that the ocean surface features observed in the IR imagery are not related to surface gravity waves (Jessup, 1996).

A warm layer model (Fairall et al., 1996), commonly used to predict the evolution of temperature very near the surface, suggests

that shear instabilities are likely during this time. Thorpe (1988) observed similar coherent structures during stable stratification that exhibited positive skewness. Here, the observed skewness is 2.8, which is significantly greater than that observed by Thorpe (1988) and strongly suggestive of "billows" due to shear-induced instability.

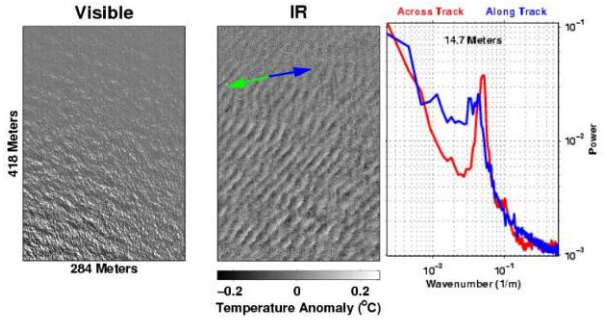


**Figure 29.** Visible image, IR image, and spectra of the IR image showing coherent ramp structures observed on August 14, 2003 in the afternoon. The wind speed (Blue Arrow) is roughly 4 m s-1 from the West and the surface current (Green Arrow) is 17 cm s-1 from the East.

For wind speeds greater than 5 $ms^{-1}$, there was significantly less spatial variability in SST, but distinct row/streak structures aligned with the wind were observed. These features are likely due to Langmuir circulation cells (Fig. 30). The horizontal spacing of these features coincided with wind-aligned surface slicks and bubbles visible in the video. The wind speed in Fig. 30 was roughly 5 $ms^{-1}$ and the surface current is 47 cm $s^{-1}$, both from the west-southwest. The IR image shows an ocean surface with thin bands of cool water that are parallel to the wind and about 0.2°C less than the regions between the bands. The dominant scale between these cool bands is 21.0 m, the features are evident throughout the CBLAST-Low region, and the distribution of temperature variability is approximately Gaussian.

The combination of a well-mixed layer with the wind and wave orientation seen in Fig. 30 provides a highly favorable environment for the development of Langmuir circulation. These structures, aligned with the wind and perpendicular to the surface waves, are suggestive of Langmuir circulation. In addition, the spacing of the cells agree well with the scale expected for Langmuir cells, given the approximately 6-m deep mixed layer observed at the moorings. These fine-scale measurements demonstrate processes that directly affect the thermal boundary layer and therefore are important to upper-ocean mixing and transport dynamics as well as the magnitude and distribution of air-sea fluxes.

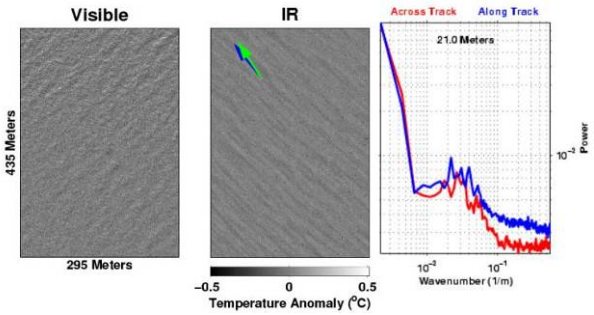


**Figure 30.** Video image, IR image, and spectra of the IR image depicting Langmuir circulation observed on August 25, 2003 in the morning. The wind speed (Blue Arrow) is roughly 5 m $s^{-1}$ and the surface current (Green Arrow) is 47 cm $s^{-1}$, both from the West-Southwest.

***Stable Boundary Layers and Fog***. As with terrestrial boundary layers, our understanding and ability to simulate processes in stratified (stable) marine ABLs lags our understanding of convective ABL processes. Over the past several decades, marine investigations have concentrated on neutral to slightly convective MABLs and our parameterizations have been tuned to these conditions (e.g., Edson et al., 2004). In contrast, oceanographers have focused on neutral to stratified boundary layer and the inherent complexity that arises due to patchy and intermittent turbulence.

The ABL over the CBLAST region was typically stable during the first half of the summer due to the combination of advection and a slowly warming coastal ocean (Crofoot 2004). This is a common occurrence along the East coast during the late spring and early summer. Stable marine ABL is also a common occurrence on the West coast, particularly when northerly winds drive

coastal upwelling. As residents of both coasts can attest, these stable MABLs are often characterized by fog and cool summertime weather.

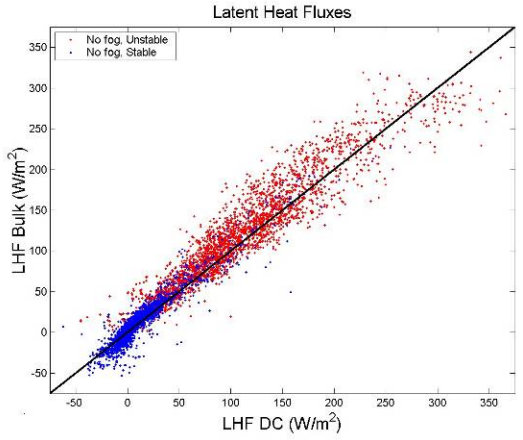


**Figure 31.** Comparison of bulk aerodynamic versus direct covariance latent heat fluxes measured from ASIT. The red dots indicate unstable conditions (i.e., positive buoyancy flux) while the blue dots indicate stable conditions (i.e., negative buoyancy flux).

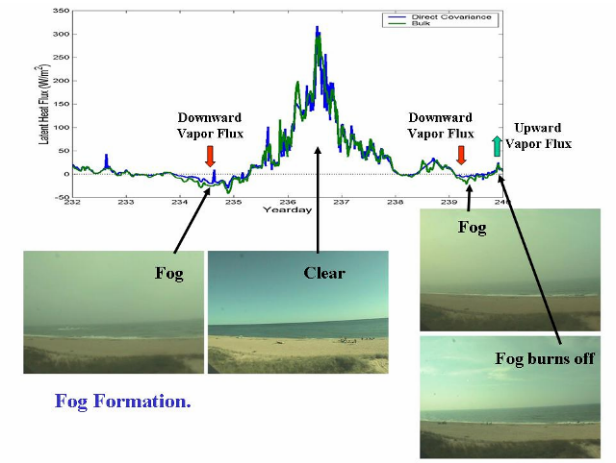


**Figure 32.** Time series of the latent heat fluxes and visual evidence for the presence of fog during periods of downward moisture flux.

The uncertainty in the determination of the momentum and scalar fluxes remains one of the main obstacles to accurate numerical forecasts in stable MABLs. For example, our initial investigations have shown significant differences between direct covariance and bulk fluxes in stable conditions, particularly when the moisture flux is directed downward (Fig. 31). These periods of downward moisture flux are often associated with foggy conditions as shown in Fig. 32. The CBLAST data indicates that the Dalton numbers remain lower than the COARE algorithm parameterization even after removal of downward fluxes and foggy periods (Fig. 33). Therefore, improvement of heat flux parameterizations in stable conditions is a main objective of ongoing investigations.

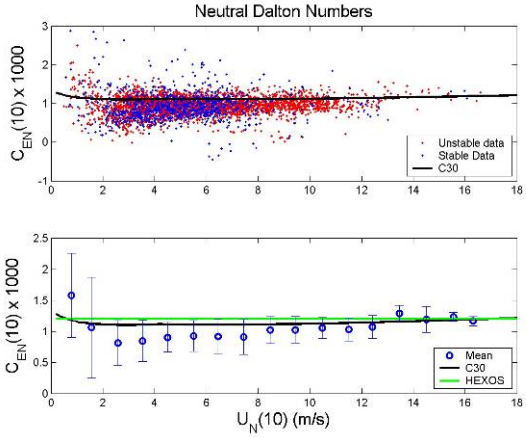


**Figure 33.** Individual and bin-averaged estimates of the neutral Dalton number. The black lines labeled with C30 represents the COARE 3.0 parameterization from Fairall et al. (2003), while the green line represents the HEXOS parameterization from DeCosmo et al. (1996).

COAMPS® analysis has shown that improved parameterizations are only part of the improvements required for accurate forecasts of fog. For example, COAMPS® runs have shown that its ability to predict fog is extremely sensitive to the SST used in the model. These sensitivity tests indicate that a 4°C increase in SST forces the model prediction to go from heavy fog to no fog as shown in Fig. 34. The strong dependence of fog formation on SST should come as no surprise. However, SST variability of several degrees is the rule rather than the exception in coastal regions where, as shown by ROMS, upwelling and lateral advection often dominate the dynamics.

Therefore, the real point of the sensitivity test was to illustrate the importance of accurate SST estimates at higher spatial and temporal resolution than is normally available,

particularly in coastal regions. One main reason for the lack of SST estimates is due to weather systems that often obscure the surface with clouds and fog, which is impenetrable to IR remote sensing. New technologies are able to peer through clouds and fog, but these suffer from low resolution and biases. Therefore, a reasonable solution to this problem is to develop a truly coupled atmosphere-ocean forecast system that provides the necessary spatial and temporal resolution, complemented with improved estimates of SST from remote and in situ observing systems. CBLAST investigations continue with this goal in mind.

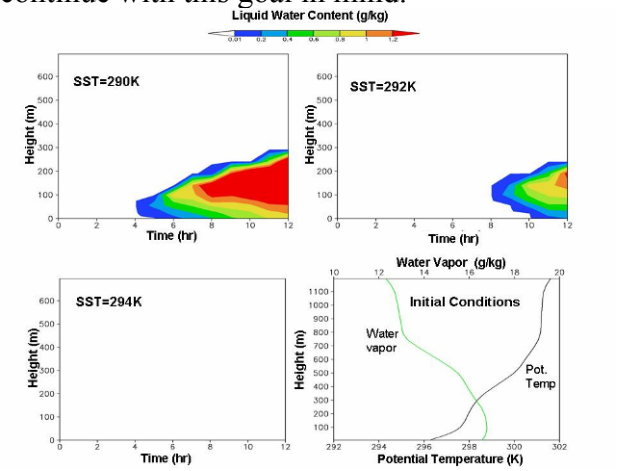


**Figure 34.** The sensitivity of fog formation to SST as indicated by model predictions of liquid water content for the 3 SSTs shown. The lower right panel shows the initial conditions in the ABL for each of the 3 runs.

**SUMMARY** An unprecedented data set was collected on both sides of the ocean-atmosphere interface during the CBLAST-LOW experiments. This included the first direct measurements of heat and momentum exchange on both sides of the air-sea interface. These measurements are being used to investigate processes that govern the exchange of momentum, heat, and mass across the coupled boundary layers. These process studies have involved close collaboration with numerical modelers and many of these investigations are guided by the numerical simulations summarized in Table 2. Our initial investigations indicate that ocean waves and wave related processes have a significant impact on air-sea exchange and coupled boundary layer processes even under light wind conditions. These studies have also shown that mesoscale and finer scale variability in the SST field strongly modulates the vertical structure of the coupled boundary layers. Continued investigations are expected to improve the predictive capabilities of a coupled air-sea models.

**In Memoriam:* This research is dedicated and in tribute to the late Dr. Timothy Crawford (1948-2002), director of the Field Research Division (FRD) of the National Oceanic and Atmospheric Administration's (NOAA) Air Resources Laboratory (ARL). Tim always stated "It's not about the flying. It's about the science." The scientific community suffered a tragic loss with his passing on August 3, 2002. He was 53 years old.

*Acknowledgements:* This work was supported by the Office of Naval Research. The manuscript was put together by the CBLAST Program Office using support from ONR grant numbers N00014-00-1-0409 and N00014-05-1-0139. Many of deployment activities for CBLAST-LOW were supported by the MVCO management team. In particular, the PIs acknowledge the support provided by Janet Fredericks, Stephen Faluotico, Margaret McElroy, and Jay Sisson.

## REFERENCES

Austin, T., J. Edson, W. McGillis, M. Purcell, R. Petitt, M. McElroy, J. Ware, C. Grant, and S Hurst, 2002: A network-based telemetry architecture developed for the Martha's Vineyard coastal observatory. *IEEE J. Oceanic Eng.*, **27**, 228-234.

Black, P. G., and Coauthors, 2007: Air-sea exchange in hurricanes: Synthesis of

observations from the coupled boundary layer air-sea transfer experiment. *Bull. Amer. Meteor. Soc.*, **88**, 357-374.

Businger, J. A., 1988: A note on the Businger-Dyer profiles. *Bound.-Layer Meteorol*., **42**, 145-151.

Chen, S. S., J. F. Price, W. Zhao, M. A. Donelan, and E. J. Walsh, 2007: The CBLAST-Hurricane Program and the next-generation fully coupled atmosphere-wave-ocean models for hurricane research and prediction *Bull. Amer. Meteor. Soc.*, **88**, 311-317.

Crofoot, R. F., 2004: Investigations of scalar transfer coefficients in fog during the Coupled Boundary Layers and Air-Sea Transfer experiment: A case study, *M.S. Thesis*, WHOI/MIT Joint Program.

D'Asaro, E.A. 2001. Turbulent vertical kinetic energy in the ocean mixed layer. *J. Phys. Oceanogr.*, **31**, 3530-3537.

D'Asaro, E.A. and G.T. Dairiki. 1997. Turbulent intensity measurements in a wind driven mixed layer. *J. Phys. Oceanogr.*, **27**, 2009-2022.

DeCosmo, J., K. B. Katsaros, S. D. Smith, R. J. Anderson, W. A. Oost, K. Bumke, and H. Chadwick, 1996: Air-sea exchange of water vapor and sensible heat: The humidity exchange of the sea experiment (HEXOS) results. *J. Geophys. Res.*, **101** (C5), 12001-12016.

Edson, J. B., C. J. Zappa, J. A. Ware, W. R. McGillis, and J. E. Hare, 2004: Scalar flux profile relationships over the open ocean. *J. Geophys. Res.*, **109**, C08S09, doi:10.1029/2003JC001960.

Fairall, C. W., E. F. Bradley, J. E. Hare, A. A. Grachev, J. B. Edson, 2003: Bulk parameterization of air–sea fluxes: Updates and verification for the COARE algorithm, *J. Climate*, **16**, 571–591.

Fairall, C.W., E.F. Bradley, J.S. Godfrey, G.A. Wick, J.B. Edson, and G.S. Young (1996), Cool-skin and warm-layer effects on sea surface temperature, *J. Geophys. Res.*, **101** (C1), 1295-1308.

Farrar, J.T., R.A. Weller, C.J. Zappa, and A.T. Jessup, Subsurface expressions of sea surface temperature variability under low winds, in *16th Symposium on Boundary Layers and Turbulence*, Ref. P8.1, Portland, Maine, USA, 2004.

Grimmett, T. K., J. R. Grench, and G. H. Crescenti, 2006: Spatial variability of CD over water in light winds measured from an instrumented aircraft. *Bound.-Layer. Meteor.*, submitted.

Hare, J.E., T. Hara, J.B. Edson, and J.M. Wilczak, 1997: A similarity analysis of the structure of air flow over surface waves. *J. Phys. Oceanogr.,* **27**, 1018-1037.

He, R. and J. L. Wilkin, 2006: Barotropic tides on the southeast New England shelf: A view from a hybrid data assimilative modeling approach. *J. Geophys. Res*, **111**, C08002, doi:10.1029/2005JC003254.

Hodur, R.M., 1997: The Naval Research Laboratory's Coupled Ocean/Atmosphere Mesoscale Prediction System (COAMPS). *Mon. Wea. Rev*., **125** 1414-1430.

Hristov, T. S., S. D. Miller, and C. A. Friehe, 2003: Dynamical coupling of wind and ocean waves through wave-induced air flow. *Nature*, **422**, 55-58.

Kaimal, J.C., J.C. Wyngaard, Y. Izumi, and O.R. Coté, 1972: Spectral characteristics of surface-layer turbulence. *Quart. J. Roy. Meteor. Soc.*, **98**, 563-589.

Katsaros, K., Radiative sensing of sea surface temperature, in *Air Sea Interaction: Instruments and Methods*, edited by F. Dobson, L. Hasse, and R. Davis, pp. 293-317, Plenum Press, New York, 1980.

Kraus, E.B. and J.S. Turner, 1967: A one-dimensional model of the seasonal thermocline. II. The general theory and its consequences. *Tellus*, **19**, 98-105.

Li, M., C. Garrett and E. Skyllingstad. 2005. A regime diagram for classifying turbulent large eddies in the upper ocean. *Deep-Sea Res. I,* **52**, 259-278.

Large, W. G., and S. Pond, 1981: Open ocean momentum flux measurements in moderate to strong winds. *J. Phys. Oceanogr.*, **11**, 324-336.

Large, W. G., J. C. McWilliams, and S. C. Doney, 1994: Ocean vertical mixing: A review and a model with a nonlocal k-profile boundary layer parameterization. *Rev. Geophys.*, **32**, 363-403.

Louis, J. F., 1979: A parametric model of vertical eddy fluxes in the atmosphere. *Bound.-Layer. Meteor.*, **17**, 187-202.

Marmorino, G.O., G.B. Smith, and G.J. Lindemann, 2004. Infrared imagery of ocean internal waves, *Geophys. Res. Lett.,* **31**, L11309, doi:10.129/2004GL020152.

Mellor, G. L., and Yamada, T., 1982: Development of a closure model of geophysical flows, *Rev. Geophys. Space Physics*, **20**, 851-875.

Osborne, M.F.M., 1965. The effect of convergent and divergent flow patterns on infrared and optical radiation from the sea, *Dt. Hydrogr. Zeitschrift* , 18, 1-25.

Plueddemann, A.J. and R.A. Weller, 1999. Structure and evolution of the oceanic surface boundary layer during the Surface Waves Processes Program, *J. Mar. Sys*., 21, 85-102

Plueddemann, A.J., E.A. Terray and R. Merewether, 2001. Design and performance of a self-contained, fan-beam ADCP, *IEEE J. Oceanic Eng*., 26(2), 252-258.

Plueddemann, A.J., J.A. Smith, D.M. Farmer, R.A. Weller, W.R. Crawford, R. Pinkel, S. Vagle and A. Gnanadesikan, 1996: Structure and variability of Langmuir circulation during the Surface Wave Processes Program. *J. Geophys. Res.*, **101** (C2), 3525-3543.

Price, J., R. Weller and R. Pinkel, 1986: Diurnal Cycling: Observations and Models of Upper Ocean Response to Diurnal Heating, Cooling and Wind Mixing., *J. Geophys. Res.,* **91**, 8411-8427.

Pritchard, M. and R.A. Weller, 2005. Observations of internal bores and waves of elevation on the New England inner continental shelf during summer 2001. *J. Geophys. Res.*, **110**, C03020, doi:10.1029/2004JC002377.

Pritchard, M., J. Gobat, W. Ostrom, J. Lord, P. Bouchard, and R. Weller, 2002: CBLAST-Low Pilot Study: Mooring deployment cruise and data report; FV Nobska, June 4 to August 17, 2001.Woods Hole Oceanographic Institution, WHOI-2002-03, 61 pp.

Pullen, J., J. D. Doyle, R. Signell, 2005: Two-way air sea coupling: A study of Adriatic. *Mon. Wea*. Rev., In press.

Skyllingstad, E.D., R. Samelson, L. Mahrt, and P. Barbour, 2005. A numerical modeling study of offshore flow over cool water. *Mon. Wea. Rev.,* **133**, 345-361.

Skyllingstad, E. D., D. Vickers, L. Mahrt, and R. Samelson, 2006: Effects of mesoscale sea-surface fronts on the marine boundary layer. *Bound.-Layer Meteor*., in press.

Smedman, A., U. Högström, H. Bergström, A. Rutgersson, K. K. Kahma, and H. Pettersson, 1999: A case study of air-sea interaction during swell conditions. *J. Geophys. Res.*, **104**, 25833-25851.

Smith, S. D., 1980: Wind stress and heat flux over the ocean in gale force winds. *J. Phys. Oceanogr.*, **10**, 709-726.

Smith, S. D., R. J. Anderson, W. A. Oost, C. Kraan, N. Maat, J. DeCosmo, K. B. Katsaros, K. L. Davidson, K. Bumke, L. Hasse and H. M. Chadwick, 1992: Sea surface wind stress and drag coefficients: The HEXOS results. *Bound.-Layer Meteorol*., **60**, 109-142.

Sullivan, P. P., et al., 2004: Large-eddy simulations and observations of wave-driven boundary layers, *16th Symp. on Boundary Layers and Turbulence*, Amer. Meteor. Soc., Portland, ME.

Thorpe, S.A. (1988), The dynamics of the boundary layers of the deep ocean, *Science Progress*, *72* (286), 189-206.

Vickers, D. and L. Mahrt, 1999: Observations of non-dimensional wind shear in the coastal zone, *Quart. J. Roy. Met. Soc.*, *125*, 2685-2702.

Vickers, D., L. Mahrt, J. Sun, and T. Crawford, 2001: The structure of offshore flow, *Mon. Wea. Rev.*, **129**, 1251-1258.

Vickers, D., and L. Mahrt, 2005: A solution for flux contamination by mesoscale motions with very weak turbulence, *Bound.-Layer Meteor.*, in press.

Vickers, D., and L. Mahrt, 2006: Evaluation of air-sea flux bulk formula and sea-surface temperature variability based on aircraft and tower observations. *J. Geophys. Res.*, **111**, doi:10.1029/2005JC003323.

Walsh, E.J., R. Pinkel, D. E. Hagan, R. A. Weller, C. W. Fairall, D. P. Rogers, S. P. burns, and M. Baumgartner, 1998. Coupling of internal waves on the main thermocline to the diurnal surface layer and sea surface temperature during the Tropical Ocean-Global Atmosphere Coupled Ocean-Atmosphere Response Experiment. *Journal of Geophysical Research, 103*, 12613-12628.

Wang, S., Q. Wang, and J. Doyle, 2002; Some improvement of Louis surface flux parameterization. *15th Symposium on Boundary layers and Turbulence*, American Meteorological Society, 15-19, July 2002, Wageningen, the Nettherland. 547-550.

Wang, S., et al., 2004: Evaluation of COAMPS™ real time forecast for CBLAST-Low summer experiments 2002/2003, *Proc. 16th Symp. on Boundary Layers and Turbulence*, Portland, ME, Amer. Meteor. Soc.

Wilkin, J., 2006: Modeling the summertime heat budget and circulation of southeast New England shelf waters, *J. Phys. Oceanogr*, **36**, 1997-2011.

Wilkin, J., and L. Lanerolle, 2005: Ocean Forecast and Analysis Models for Coastal Observatories, in *Ocean Weather Forecasting: An Integrated View of Oceanography*, E. Chassignet and J. Verron, Eds., Springer, 549-572.

Zappa, C.J., and A.T. Jessup, 2005: High resolution airborne infrared measurements of ocean skin temperature, *Geoscience and Remote Sensing Letters*, ***2*** (2), doi:10.1109/LGRS.2004.841629.

| **Table 1. Instrumentation deployed on and around ASIT during the 2003 IOP.** | | | |
|---|---|---|---|
| Sensors | Variables | Location on Fig. 6 | Nominal Measurement height(s) |
| Pyrgeometer | IR radiative flux | A | 22 m |
| Pyranometer | Solar radiative flux | A | 22 m |
| Sonic Anemometer | Fast response 3-component velocity, temperature | B, C, D | 20, 18, 15 m |
| Rain Gauge | Precipitation | D | 13 m |
| Pressure sensor | Mean pressure. | C, F, G, I | 18, 10, 9, 6.5 m |
| T/RH sensor | Mean temperature, relative humidity | B, C, D, G, H, J | 21, 18, 13.5, 9, 7, 5 m |
| Sonic anemometer, infrared hygrometer | Fast response 3-component velocity, temperature, water vapor | F, I, K | 10, 6.5, 4 m |
| Static pressure sensor | Fast response static pressure | F, I | 10, 6.5 m |
| Profiling package: T/RH sensor, sonic anemometer | Mean Temperature, relative humidity, horizontal velocity | L | 2.5 to 16 m |
| Radiometer | Sea surface temperature | E | 0 m |
| Laser altimeter, microwave altimeter | Surface elevation, wave height | E | 0 m |
| Microwave altimeter | Surface elevation, wave height | E | 0 m |
| Fanbeam ADCP | 2-D maps of surface velocities | Seafloor | 0 m |
| High resolution acoustic Doppler current profiler (ADCP) | Current profiles | S (end of beam) | -3.5 to 0 m |
| Acoustic Doppler Velocimeter (ADV), thermistor | Fast response 3-component velocity and temperature | N, P | -3.5 m |
| Acoustic Doppler Velocimeter (ADV) | Fast response 3-component velocity | M, Q, R | -3.5 m |
| Acoustic Doppler Velocimeter (ADV), pressure | Fast response 3-component velocity, wave height and direction | S (end of beam) | -3.5 m |
| Conductively, temperature, depth (CTD) sensor | Salinity, temperature, depth | O & Seafloor | -1.5, -5, -12 m |
| Broadband Acoustic Doppler Current Profiler (BADCP) | Current profiles, vertical velocity profile | Seafloor | -13 to -0.5 m |
| Acoustic Doppler current profiler (ADCP) | Current profiles | Seafloor | -13 to -0.5 m |
| Current meter | Fast response 3-component velocity | Seafloor | -12 m |

| **Table 2. Simulations Studies Conducted in Support of CBLAST.** | | |
|---|---|---|
| Study | Simulation | PI(s) |
| Turbulence airflow over swell and its impact on wave boundary layer structure. | Atmospheric LES with BC conditions imposed by resolved waves (swell) and parameterized surface roughness. | P. Sullivan, J. Edson, J. McWilliams, T. Hristov |
| Simulations of atmospheric boundary layer in CBLAST region. | Atmospheric LES using boundary conditions from COAMPS® mesoscale model | P. Sullivan, S. Wang |
| Simulation of atmospheric boundary layer evolution over mesoscale SST fronts. | Atmospheric LES over step changes in sea surface temperature. | E. Skyllingstad, L. Mahrt, D. Vickers |
| Detailed studies of the coupling mechanisms between the air and water turbulent flows. | DNS using fully-nonlinear free-surface coupled boundary conditions | D.K.P. Yue, L. Shen |
| Simulations of the effect of wave breaking on the ocean surface layer | Oceanic DNS with stochastic wave breaking. | P. Sullivan, J. McWilliams, K. Melville |
| Impacts of breaking waves and Langmuir circulation on the ocean mixed layer | Ocean LES with Craik-Leibovich vortex force and intermittent stress transmission from a spectrum of breaking wave events | P. Sullivan, J. McWilliams, K. Melville |
| Deepening of the ocean mixed layer by Langmuir and shear turbulence | Stratified ocean LES with Craik-Leibovich vortex force and constant surface stress | M. Li, A. Plueddemann |